arXiv:1812.02221v2 [physics.flu-dyn] 1 Jun 2019

Broadband Wall-less Waveguide for Shallow Water Waves

Ahmad Zareei* and Mohammad-Reza Alam

Mechanical Engineering Department, University of California, Berkeley 94720, USA

We present a broadband waveguide for water waves obtained through mere manipulation of seabed properties and without any need for sidewalls. Specifically, we show that a viscoelastic seabed results in a modified effective gravity term in the governing equations of water waves, which provides a generic broadband mechanism to control oceanic wave energy and enables confining surface waves inside a long narrow path without sidewalls. Our findings have promising applications in guiding and steering waves for oceanic wave energy farms or protecting shorelines.

INTRODUCTION

The Intensity of all physical waves decreases as they propagate away from their sources due to the so-called spreading loss. Waveguides counteract this spreading and keep the energy flowing over long distances with minimal losses. The simplest waveguide is based on reflection of waves from waveguide's boundary due to a sharp change in refractive index [1-3]. For electromagnetic waves, optical fibers (or dielectric slabs) are an example of such waveguides where light rays entering the fiber with incidence angle up to the fiber's cut-off angle [4] get reflected from boundaries, stay confined, and propagate inside the fiber [5]. An equivalent of such simple waveguide for water waves is a side-wall confinement where water waves propagate inside a *canal* while getting reflected from boundaries. Additionally, the propagation dynamics of various surface gravity water wave envelopes in canals has been extensively studied [6-8].

The drawback of reflection-based waveguides is modal dispersion which effectively spreads the temporal duration of a pulse and limits the operational bandwidth [9]. Modal dispersion may considerably be reduced by engineering the velocity profile and therefore the refractive index distribution inside a waveguide. A graded core fiber with a parabolic refractive index profile [10] is an example of such waveguides for electromagnetic waves, where wave rays refract toward the fiber's centerline as they travel through the waveguide [11–14]. Shallow water waves behave similar to optical waves, where water wavenumber k is equivalent to optical refractive index n and it satisfies the Fermat's principle similar to optics [15]. The wavenumber in surface gravity waves depends on the water depth and gravitational acceleration through $c^2 = gh$, where $c = \omega/k$ is the phase speed, g is the gravitational acceleration, and h is the water depth. As a result, any variation in water depth or gravitational acceleration alters the refractive index profile which would enable wave ray path engineering in water waves, e.g., a ridge-form sea-bed topography has a refractive index similar to a graded-index fiber and is capable of trapping certain frequencies of long-wave oceanic waves over the ridge [16, 17]. Besides refractive index, the effects of depth variation on water wave propagation can be considered through other mechanisms as well, e.g., through (i) Bragg resonance between surface waves and sea-bed topography [18–20]; (ii) band features of periodic structures inspired by photonic crystals [21–27]; (iii) homogenization effect of a rapidly changing topography [28–31]. The first two methods are narrow band and highly sensitive to frequency, while the last approach works in a broader range of frequencies. The effective bandwidth of last approach, the homogenization method, can be found by homogenization condition which restricts the incident wavelength to be much larger than characteristic length of sea-bed variations.

The other parameter affecting water waves, in addition to water depth, is the gravitational acceleration which on the contrary is always a physical constant and can not be altered. While the actual gravity is constant, the observed effective gravity can change. There are only a few studies observing an altered effective gravitational acceleration for water waves: (i) an array of vertical cylinders at low frequencies simultaneously changes both effective depth and effective gravity which depends on the filling ratio of cylinders [32]; (ii) a periodic array of resonators at low frequencies has a negative effective gravity which results in band-gap that strongly reflects the waves [33, 34]; (iii) a thick, rigid, and unmovable plate covering the water surface exhibits an infinite gravitational acceleration (or equivalently a zero refractive index) which is analogous to epsilon near zero materials in optics [35–37] and has potential applications in focusing and collimation of water waves [38]. Although these methods offer scenarios in which an altered effective gravitational acceleration is observed (only infinite or negative); they do not provide a generic mechanism to obtain finite variations in effective gravitational acceleration. It is to be noted that arbitrary modification of effective gravity enables broadband manipulation of shallow water waves which, on the contrary, is not possible through water depth variations. Furthermore, the transformation optics method usually requires variations in the gravitational acceleration [30] which enforces using alternative methods [e.g., 39, 40].

Here, we show that a visco-elastic bottom topography results in an effective gravitational acceleration which can be adjusted through elasticity and damping of a sea-bed carpet. The tunable effective gravitational acceleration provides a generic mechanism to control the flow of ocean wave energy through a passive sea-bed, and is exemplified by a water waveguide which has no physical walls and still confines the water waves to propagate inside the waveguide region. The water waveguide is analogous to graded index optical fibers with parabolic refractive index and is engineered through the effective gravitational acceleration using elastic sea-bed carpet. Water waves over the designed elastic sea-bed (waveguide) are transmitted over long distances with a low attenuation loss. We numerically validate the design and test the effectiveness of the waveguide in transmitting water wave energy. The proposed mechanism along with water depth variations open new venues in the control of ocean wave energy which have engineering applications in guiding and steering incoming waves toward or away from destinations of interest such as artificial surf zones, wave energy farms, or to protect shorelines.

GOVERNING EQUATIONS

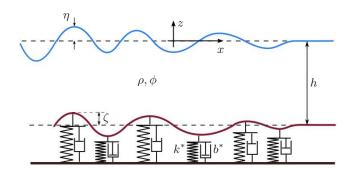


FIG. 1. Schematic of a visco-elastic carpet on the seafloor. The carpet is composed of linear springs with stiffness coefficient k^* providing the restoring force, and dash-pot type dampers with damping coefficient b^* extracting energy from the system. The distance between each module of the spring damper is assumed to be much smaller than the typical wavelength of the over passing waves such that the assumption of continuously distributed springs and dampers is valid.

We consider an inviscid, incompressible, and irrotational fluid over a visco-elastic sea-bed (see Fig. 1). We set the coordinate system on the mean free surface of water with z-axis pointing upward and the mean depth being at z = -h. The linearized governing equations for the surface/bottom elevation η/ζ and the velocity potential ϕ , ignoring the surface tension, are [41]

$$\nabla^2 \phi = 0, \qquad -h \le z \le 0 \tag{1a}$$

$$\eta_t = \phi_z, \qquad z = 0 \tag{1b}$$

$$\phi_t + g\eta = 0, \qquad z = 0 \tag{1c}$$

$$\zeta_t - (h_x \phi_x + h_y \phi_y) = \phi_z, \quad z = -h \tag{1d}$$

$$\phi_t + g\zeta + \frac{1}{\rho} [b^* \zeta_t + k^* \zeta] = 0, \quad z = -h$$
 (1e)

where k^* and b^* are the stiffness and viscous damping coefficient of the visco-elastic bottom per unit area, ρ is the density of fluid, and g is the gravitational acceleration. In this set of governing equations, (1a) is the continuity equation in the fluid domain, (1b) and (1d) are the kinematic boundary conditions on the free surface and bottom topography, and (1c) and (1e) are dynamic boundary conditions on the free surface and visco-elactic bottom. We nondimensionalize the governing equations with the following nondimensional groups as

$$(x', y') = k(x, y), \quad z' = \frac{z}{H}, \quad h' = \frac{h}{H}, \quad t' = k\sqrt{gHt},$$
(2a)

$$\eta' = \frac{\eta}{A}, \quad \phi' = \left(\frac{1}{k}\frac{A}{H}\sqrt{gH}\right)^{-1}\phi$$
 (2b)

$$\zeta' = \frac{\zeta}{A}, \quad \lambda = (kH) \frac{b^*}{\rho \sqrt{gH}}, \quad \gamma = \frac{k^*}{\rho g}, \quad \mu \equiv kh$$
 (2c)

where k and A are respectively the characteristic wave number and wave amplitude of incident waves. Nondimensionalizing the governing equations in (1), dropping the primes for the sake of simplicity, and assuming of time harmonicity ω for the incoming waves, the governing equations simplify to

$$\mu^{2} \left(\phi_{xx} + \phi_{yy} \right) + \phi_{zz} = 0, -h \le z \le 0$$
 (3a)

$$-\mu^2 \omega^2 \phi + \phi_z = 0, \qquad z = 0 \tag{3b}$$

$$\mu^2 \frac{\omega^2 \phi}{1 + \lambda(i\omega) + \gamma} - \mu^2 \left(h_x \phi_x + h_y \phi_y \right) = \phi_z, \qquad z = -h.$$

Next, we assume the shallow water regime, $\mu \ll 1$, and expand the solution for the velocity potential as $\phi = \phi^{(0)} + \mu^2 \phi^{(2)} + \ldots$ Finding the zeroth and second order solutions, and considering the solvability condition [15], one can obtain the zeroth mode governing equation. In the dimensional form, the governing equation reads

$$\nabla \cdot \left(h\nabla\phi^{(0)}\right) + \frac{\omega^2}{\tilde{g}}\phi^{(0)} = 0, \qquad \tilde{g} = g\left[1 + \frac{\rho g}{k^* + \mathrm{i}b^*\omega}\right].$$
(4)

The obtained governing equation (4) is similar to the shallow water wave equation [15]; however, with a different gravitational acceleration \tilde{g} . This derivation suggests that the net effect of a visco-elastic sea-bed in shallow water regime can be summarized with a modified gravity term that depends on the elasticity and viscosity of the sea-bed.

BROADBAND WAVEGUIDE DESIGN

In an incompressible, inviscid, and irrotational fluid where the fluid depth is h, the wave equation in long wave limit $kh \ll 1$ reads as $\nabla (h\nabla \phi) + \omega^2 \phi/g = 0$, where ∇ is the horizontal gradient, ϕ is the velocity potential with fluid velocity $\mathbf{v} = \nabla \phi$, ω is the wave frequency, and g is the gravitational acceleration. Equivalent refractive index for water waves is obtained as $n = c_0/c$, where c_0 is the wave phase velocity at a reference point and c is the local phase velocity [15]. Since phase velocity is inversely proportional to the wave number, $c = \omega/k$, the refractive index becomes proportional to the wave number as $n \propto k$. Phase velocity of shallow water waves depends on the water depth and gravitational acceleration through $c = \sqrt{gh}$, where variations in water depth h, or gravitational acceleration g would lead to changes in the refractive index n. The local refractive index determines the wave ray paths for water waves, and therefore enables steering of water waves through refractive index profile engineering. In shallow water waves, water depth is constrained by $kh \ll 1$, and as a result water depth variation decreases the effective bandwidth of the system. The only other parameter that effects the refractive index is the gravitational acceleration which is a physical constant. Nevertheless, a visco-elastic sea-bed results in an effective (modified) gravitational acceleration which can be adjusted by changing the elasticity and viscosity of the sea-bed. The modified gravitational acceleration allows variations in refractive index and contrary to water depth variations does not restrict the effective bandwidth of the system.

Assuming a visco-elastic sea-bed, the governing equation for shallow water waves is obtained as $\nabla .(h\nabla \phi) + \omega^2 \phi/\tilde{g} = 0$, where

$$\tilde{g} = g \left[1 + \frac{\rho g}{k^* + \mathrm{i}b^*\omega} \right],\tag{5}$$

in which k^*, b^* are the spring and damping coefficient of the visco-elastic bottom, ρ is the fluids density, and ω is the frequency of incoming wave. Therefore, the effective gravitational acceleration observed is different from constant gravitational acceleration g and can be altered using stiffness and damper coefficients in the viscoelastic sea-bed. In the limit where the springs are stiff $k^*/\rho g \gg 1$, the effective gravitational acceleration simplifies to $\tilde{g} = g$ as expected. The imaginary part of the effective gravitational acceleration depends on both frequency and damper coefficient $ib^*\omega$ and represents the absorption of energy by the dampers in the visco-elastic carpet and can be used in designing high-performance wave energy extraction devices through actuated seafloor mounted carpets [41, 42].

Using obtained effective gravity in (5), the refractive index becomes

$$n = \frac{c_0}{\sqrt{\tilde{g}h}} = \sqrt{\frac{h_0}{h}} \frac{1}{\sqrt{1 + \rho g/\left(k^* + ib^*\omega\right)}},$$
 (6)

where it depends on the visco-elastic sea-bed parameters. This provides a generic broadband mechanism to alter the refractive index through elasticity and viscosity of the sea-bed, and hence enables control of wave rays path of oceanic water waves. Here as an example, we design a visco-elastic sea-bed analogous to graded-index optical fibers for guiding water waves.

Graded-index waveguides (or fibers) in optics are used to guide electromagnetic waves over long distances. The refractive index of such waveguides should vary as $n(y) = n_c \operatorname{sech}(\kappa y/L)$, where n(y) is the refractive index of the waveguide measured by the distance from the center line of the fiber, n_c is the fiber's core refractive index, L is the width of the waveguide, and κ is a tuning parameter that controls the distance between focal points L_f (Fig. 2).

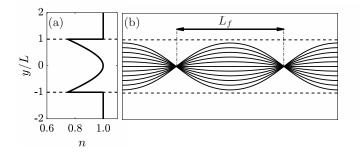


FIG. 2. (a) Refractive index profile in a graded index (GRIN) wave guide where $n(y) = n_c \operatorname{sech}(\kappa y/L)$. (b) Top view of ray paths (solid lines) in a graded-index wave-guide (dashed lines). The tuning parameter κ in refractive index profile controls the distance between focal points L_f .

For the ease of experiment, we use the first two terms in the Taylor expansion of refractive index as [43]

$$\left(\frac{n(y)}{n_c}\right)^2 = 1 - \delta \frac{y^2}{L^2},\tag{7}$$

which gives a parabolic refractive index profile with $\delta = \kappa^2$. Similar to optical waves, shallow water waves stay confined inside a region with parabolic refractive index profile and wave energy is transmitted over long distances preventing the spreading loss. We take x-axis to be the center-line of the GRIN waveguide, and y-axis representing the distance from waveguide's centerline. Using equations (6) and (7), the effective gravity is obtained as $g(y) = \tilde{g}_c / (1 - \delta y^2 / L^2)$ where \tilde{g}_c represents the effective gravity at the waveguide's centerline. The stiffness of the elastic bottom topography is then obtained using equation (5) as $\rho g/k^* = \tilde{g}/g - 1$. Figure 3 depicts the values of effective gravitational acceleration and elastic sea-bed stiffness over the width of the waveguide. The profiles are plotted for different values of δ to show the sensitivity of the obtained profile with variations in δ . The waveguide's core effective gravity is considered to be very close to the gravitational acceleration $\tilde{g}_c/g = 1.001$ which translates into a stiff (or rigid) sea-bed. Note that a higher difference between core's effective gravitational acceleration

and the actual gravity causes more impedance mismatch at the entrance of the waveguide and therefore a higher reflection at the entry of the waveguide; accordingly the core's gravity is considered to be close to the actual gravity. In the asymptotic, the rigid ground has stiffness of infinity where the effective gravitational acceleration becomes the actual gravity $\tilde{g} = q$.

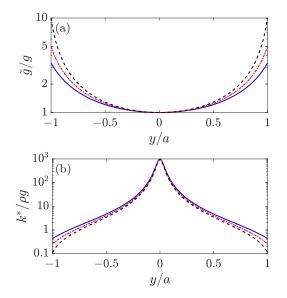


FIG. 3. Nondimensionalized stiffness $k^*/\rho g$ and effective gravity \tilde{g}/g over the width of the water waveguide y/a for different values of δ ($\delta = 0.7$ (---), $\delta = 0.8$ (---), and $\delta = 0.9$ (---)) where the waveguide's core effective gravity is considered to be very close to the gravitational acceleration $\tilde{g}/g = 1.001$

RESULTS

In order to validate the theoretical design, we use Finite Element Methods (FEM) to solve the governing equation, given the stiffness profile shown in Fig. 3 for $\delta = 0.8$. We use Crank-Nicolson method for time discretization along with piece-wise linear isoparametric shape functions for spatial discretization. We chose the open-source finite element package FreeFEM++ [44] to solve the discretized variational formulation of the governing equation. The length scale is non-dimensionalized using the wave-length of the incoming wave, and the nondimensionalized time is obtained from dispersion relation. The numerical domain is set to $[0, 30] \times [-7.5, 7.5]$, where the center of the wave guide is at y = 0 and spans in the y-direction from -1.5 to 1.5. The domain's border is seeded by $\delta x = 0.04$ and the element mesh is then created using FreeFem++ mesh generator. Waves are inserted through the waveguide using a tanh ramp-function representing the wave generator and solution is found by marching in time with $\delta t = T/100$ where T is the wave period. Artificial absorbing boundary condition is used to absorb the outgoing waves at the boundaries of the domain.

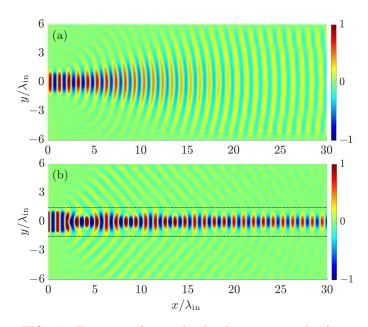


FIG. 4. Top view of normalized velocity potential $\phi/\phi_{\rm in}$, where $\phi_{\rm in}$ is the incident velocity potential inside the test region. The normalized wave amplitude profile $\eta/\eta_{\rm in}$ is the same as normalized velocity potential, since $\eta = i\omega\phi/g$. Waves are inserted in the domain from left and propagate to right. Figure (a) shows the normalized velocity potential over a constant depth sea-bed and gravity. The waves spread as they propagate and the amplitude of decreases. Figure (b) shows the normalized velocity potential when the elastic waveguide is implemented in the middle region between dashed lines (- -). The elastic sea-bed confines the waves inside the middle region and prevents the waves from spreading. The net effect of the elastic sea-bed is similar to the graded-index optical fibers that confine and transmit electromagnetic wave rays.

As shown in Fig. 4a, when the bottom topography is flat, the water waves disperse in the transverse direction normal to the wave rays propagation and therefore the wave amplitude decreases as it propagates through the simulation region. On the other hand, when the graded index waveguide is implemented through elastic sea-bed, the water waves stay confined inside the waveguide region and propagate with much less decrease in the wave's amplitude (Fig. 4b). It is to be noted that there is no physical wall at the boundaries of the waveguide, and the elastic sea-bed is only counteracting the spreading of waves which allows long distance propagation and transmission of wave energy.

In order to quantify the performance of the waveguide, the surface wave amplitude along the center line of the waveguide y = 0 is plotted in Fig. 5a. The wave amplitude at the centerline of the waveguide when the bottom topography is flat has 80% reduction due to spreading $(\eta_{\rm out}/\eta_{\rm in}=0.2)$ as it travels the distance of the waveguide $D = 30\lambda_{\rm in}$ where $\lambda_{\rm in}$ is the incident wavelength. On the contrary, waves inside the graded refractive index elastic sea-bed waveguide has only an amplitude decrease of 20% reduction with $\eta_{out}/\eta_{in} = 0.8$ (Fig. 5a). Running the simulation for an even larger domain, $D/\lambda_{in} = 35$, we observe a 90% reduction for the case of flat topography and 25% reduction for the waveguide with elastic seabed. In order to capture the motion of elastic seabed, the elastic sea-bed elevation is plotted in Fig. 5b. As shown in this figure, the amplitude of the elastic carpet is at most 7% of the incident wave amplitude, which makes it suitable for practical applications. Note that increasing the value of δ as shown in Fig. 3, would increase the values of effective gravity at the boundaries. This would decrease the amount of energy escaped from the boundaries of the waveguide and therefore increase the final magnitude of the surface elevation at the final point.

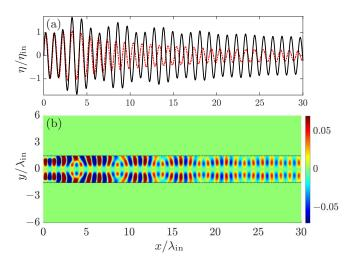


FIG. 5. (a) Wave amplitude along the center-line of numerical domain y = 0 for the case with designed sea-bed carpet (----) and flat sea-bed (- - -). (b) Normalized elevation of the elastic sea-bed carpet $\zeta/\eta_{\rm in}$. The elastic sea-bed domain is $[0, 30] \times [-1.5, 1.5]$ over which the elevation is nonzero. The maximum elevation recorded over the sea-bed is $\zeta_{\rm max}/\eta_{\rm in} = 0.07$.

CONCLUSION

In this manuscript, we showed that the net effect of a visco-elastic sea-bed can be summarized through an effective (modified) gravitational acceleration term which is adjustable through elasticity and viscosity of the sea-bed parameters. This method proposes a generic broadband mechanism for modifying the effective gravitational acceleration which enables new ways of controlling oceanic wave energy. As an example, we designed a passive elastic sea-bed which is capable of guiding and transmitting water waves over long distances. The proposed method has potential applications in guiding and steering waves toward or away from destinations of interest such as artificial surf zones, wave energy farms, or to protect shorelines.

- * zareei@berkeley.edu; Mechanical Engineering Department, University of California, Berkeley 94720, USA
- [1] J. J. Thomson, Mercury 8, 18 (1893).
- [2] L. Rayleigh, The London, Edinburgh, and Dublin Philosophical Magazine and Journal of Science 43, 125 (1897).
- [3] J. W. S. B. Rayleigh, The theory of sound, Vol. 2 (Macmillan, 1896).
- [4] F. A. Jenkins and H. E. White, Fundamentals of optics (Tata McGraw-Hill Education, 1937).
- [5] G. Keiser, Optical fiber communications (Wiley Online Library, 2003).
- [6] S. Fu, Y. Tsur, J. Zhou, L. Shemer, and A. Arie, Physical review letters 115, 254501 (2015).
- [7] S. Fu, Y. Tsur, J. Zhou, L. Shemer, and A. Arie, Physical review letters 115, 034501 (2015).
- [8] S. Fu, J. Zhou, Y. Li, L. Shemer, and A. Arie, Physical review letters 118, 144501 (2017).
- [9] C. R. Pollock and M. Lipson, *Integrated photonics*, Vol. 20 (Springer, 2003).
- [10] M. J. Adams, An introduction to optical waveguides, Vol. 14 (Wiley New York, 1981).
- [11] M. Feit and J. Fleck, Applied optics 17, 3990 (1978).
- [12] A. Zareei, A. Darabi, M. J. Leamy, and M.-R. Alam, Applied Physics Letters **112**, 023901 (2018), https://doi.org/10.1063/1.5008576.
- Conroy, [13] D. Wolfe, S. В. R., Ρ. Garstecki. Τ. Mayers, М. Α. Fischbach, Κ. В. E. M. Prentiss, Paul, and G. М. Whitesides. Proceedings of the National Academy of Sciences 101, 12434 (2004)
- [14] D. Ansell, I. Radko, Z. Han, F. Rodriguez, S. Bozhevolnyi, and A. Grigorenko, Nature communications 6, 8846 (2015).
- [15] C. C. Mei, M. Stiassnie, and D. K.-P. Yue, Theory and Applications of Ocean Surface Waves: Part 1: Linear Aspects Part 2: Nonlinear Aspects (World Scientific, 1989).
- [16] V. Buchwald, Proc. R. Soc. Lond. A 308, 343 (1969).
- [17] C. C. Mei, M. Stiassnie, and D. K.-P. Yue, *Theory and Applications of Ocean Surface Waves: Part 1: Linear Aspects Part 2: Nonlinear Aspects* (World Scientific, 1989).
- [18] Y. LIU and D. K. P. YUE, Journal of Fluid Mechanics 356, 297326 (1998).
- [19] M.-R. Alam, Y. Lie, and D. K. P. Yue, Journal of Fluid Mechanics 643, 437447 (2010).
- [20] R. B. Elandt, M. Shakeri, and M.-R. Alam, Phys. Rev. E 89, 023012 (2014).
- [21] X. Hu, Y. Shen, X. Liu, R. Fu, J. Zi, X. Jiang, and S. Feng, Phys. Rev. E 68, 037301 (2003).
- [22] X. Hu, Y. Shen, X. Liu, R. Fu, and J. Zi, Phys. Rev. E 68, 066308 (2003).
- [23] X. Hu, Y. Shen, X. Liu, R. Fu, and J. Zi, Phys. Rev. E 69, 030201 (2004).

- [24] T. S. Jeong, J.-E. Kim, H. Y. Park, and I.-W. Lee, Applied Physics Letters 85, 1645 (2004), https://doi.org/10.1063/1.1787941.
- [25] Y. Shen, K. Chen, Y. Chen, X. Liu, and J. Zi, Phys. Rev. E 71, 036301 (2005).
- [26] Y. Shen, X. Liu, Y. Tang, Y. Chen, and J. Zi, Journal of Physics: Condensed Matter 17, L287 (2005).
- [27] T. Bobinski, A. Eddi, P. Petitjeans, A. Maurel, and V. Pagneux, Applied Physics Letters 107, 014101 (2015), https://doi.org/10.1063/1.4926362.
- [28] C. P. Berraquero, A. Maurel, P. Petitjeans, and V. Pagneux, Phys. Rev. E 88, 051002 (2013).
- [29] A. Maurel, J.-J. Marigo, P. Cobelli, P. Petitjeans, and V. Pagneux, Physical Review B 96, 134310 (2017).
- [30] A. Zareei and M.-R. Alam, Journal of Fluid Mechanics **778**, 273287 (2015).
- [31] A. Zareei and M.-R. Alam, Phys. Rev. E **95**, 063002 (2017).
- [32] X. Hu and C. T. Chan, Phys. Rev. Lett. **95**, 154501 (2005).
- [33] X. Hu, C. T. Chan, K.-M. Ho, and J. Zi, Phys. Rev. Lett. 106, 174501 (2011).
- [34] X. Hu, J. Yang, J. Zi, C. T. Chan, and K.-M. Ho, Scientific reports 3, 1916 (2013).
- [35] B. Edwards, A. Alù, M. E. Young, M. Silveirinha, and N. Engheta, Phys. Rev. Lett. **100**, 033903 (2008).
- [36] R. Maas, J. Parsons, N. Engheta, and A. Polman, Nature Photonics 7, nphoton (2013).

- [37] P. Moitra, Y. Yang, Z. Anderson, I. I. Kravchenko, D. P. Briggs, and J. Valentine, Nature Photonics 7, 791 (2013).
- [38] C. Zhang, C.-T. Chan, and X. Hu, Scientific reports 4, 6979 (2014).
- [39] C. Li, L. Xu, L. Zhu, S. Zou, Q. H. Liu, Z. Wang, and H. Chen, Physical Review Letters **121**, 104501 (2018).
- [40] A. Zareei and R. Alam, in Proc. 31st Int. Workshop on Water Waves and Floating Bodies, Michigan, USA (2016) pp. 197–200.
- [41] M.-R. Alam, Proceedings of the Royal Society of London A: Mathem
- [42] N. Desmars, J. Tchoufag, D. Younesian, and M.-R. Alam, Journal of Fluids and Structures 81, 673 (2018).
- [43] C. Gomez-Reino, M. V. Perez, and C. Bao, Gradientindex optics: fundamentals and applications (Springer Science & Business Media, 2012).
- [44] F. Hecht, J. Numer. Math. **20**, 251 (2012).
- [45] A. Mehrvarz, A. Najafi Ardekani, M. J. Khodaei, and N. Jalili, Journal of Vibration and Control 25, 1393 (2019).
- [46] A. N. Ardekany and A. Mehrvarz, in 2016 4th International Conference on Robotics and Mechatronics (ICROM) (IEEE, 2016) pp. 285–288.
- [47] A. N. Ardekany, F. Daneshmand, and A. Mehrvarz, Iranian Journal of Science and Technology, Transactions of Mechanical Engineering, 1 (2018).
- [48] M. J. Khodaei, A. Mehrvarz, N. Candelino, and N. Jalili, in ASME 2018 Dynamic Systems and Control Conference (American Society of Mechanical Engineers, 2018) pp. V003T42A004–V003T42A004.